Geophysical Research Letters

RESEARCH LETTER
10.1029/2023GL103107

Identifying the Deep-Inflow Mixing Features in Orographically-Locked Diurnal Convection

Yu-Hung Chang[1], Wei-Ting Chen[1], Chien-Ming Wu[1], Yi-Hung Kuo[2,3], and J. David Neelin[3]

[1]Department of Atmospheric Sciences, National Taiwan University, Taipei, Taiwan, [2]Cooperative Institute for Modeling the Earth System, Princeton University, Princeton, NJ, USA, [3]Department of Atmospheric and Oceanic Sciences, University of California, Los Angeles, Los Angeles, CA, USA

Key Points:

- In TaiwanVVM simulations, the convective updraft structure of orographically-locked diurnal convection exhibits a deep layer of inflow
- The terrain-constrained path of coherent inflow layer by local circulation augments convection development over the precipitation hotspots
- Initial field observations guided by TaiwanVVM detect high moist static energy transport upstream of the precipitation hotspots

Correspondence to:
W.-T. Chen,
weitingc@ntu.edu.tw

Citation:
Chang, Y.-H., Chen, W.-T., Wu, C.-M., Kuo, Y.-H., & Neelin, J. D. (2023). Identifying the deep-inflow mixing features in orographically-locked diurnal convection. *Geophysical Research Letters*, *50*, e2023GL103107. https://doi.org/10.1029/2023GL103107

Received 1 FEB 2023
Accepted 5 MAY 2023

Author Contributions:
Conceptualization: Yu-Hung Chang, Wei-Ting Chen, Chien-Ming Wu, Yi-Hung Kuo, J. David Neelin
Data curation: Yu-Hung Chang
Formal analysis: Yu-Hung Chang
Funding acquisition: Wei-Ting Chen
Investigation: Yu-Hung Chang, Wei-Ting Chen, Chien-Ming Wu, Yi-Hung Kuo, J. David Neelin
Methodology: Yu-Hung Chang, Wei-Ting Chen, Chien-Ming Wu, Yi-Hung Kuo, J. David Neelin
Project Administration: Wei-Ting Chen
Resources: Wei-Ting Chen, Chien-Ming Wu
Software: Chien-Ming Wu
Supervision: Wei-Ting Chen
Validation: Yu-Hung Chang

Abstract Orographically-locked diurnal convection involves interactions between local circulation and the thermodynamic environment of convection. Here, the relationships of convective updraft structures over orographic precipitation hotspots and their upstream environment in the TaiwanVVM large-eddy simulations are analyzed for the occurrence of the orographic locking features. Strong convective updraft columns within heavily precipitating, organized systems exhibit a mass flux profile gradually increasing with height through a deep lower-tropospheric inflow layer. Enhanced convective development is associated with higher upstream moist static energy (MSE) transport through this deep-inflow layer via local circulation, augmenting the rain rate by 36% in precipitation hotspots. The simulations provide practical guidance for targeted observations within the most common deep-inflow path. Preliminary field measurements support the presence of high MSE transport within the deep-inflow layer when organized convection occurs at the hotspot. Orographically-locked convection facilitate both modeling and field campaign design to examine the general properties of active deep convection.

Plain Language Summary Under the weather regime that favors the development of local circulation in summer, diurnal convection occurs over specific areas of Taiwan. To investigate this orographic locking feature of diurnal convection, we performed a set of simulations with realistic complex Taiwan topography by TaiwanVVM and initiated with radiosonde observations to represent the variability of the background environment. In the simulations, strong updrafts are identified for orographically-locked diurnal convection over precipitation hotspots. The vertical air mass transport of heavily-precipitating updrafts increases with height throughout the lower atmosphere, implying a lateral inflow. The analysis of local circulation confirms the presence of the inflow layer, enhancing the development of orographically-locked diurnal convection via rich energy transport from upstream. A field campaign, guided by the simulations, released the Storm Tracker mini-radiosondes to quantify the upstream environment of the most common deep-inflow path on 26 August 2022. The initial analysis supports the existence of high energy transport within the inflow layer when diurnal convection occurs over the precipitation hotspot. The results highlight the importance of non-local inflow, transporting energy through the local circulation to supply the growth of orographically-locked diurnal convection.

1. Introduction

In the tropics, deep moist convection contributes to precipitation and redistributes the energy and momentum within the Earth system (Houze, 2004). Over tropical land in summer monsoon regions, convective rainfall peaking in the afternoon is a fundamental mode of precipitation variability (Nesbitt & Zipser, 2003; Yang & Slingo, 2001). Organized diurnal convection is critical to short-duration rainfall extremes in these regions and, therefore, has been intensively investigated (e.g., P.-J. Chen et al., 2021; X. Chen et al., 2015; Jian et al., 2021; Krishna et al., 2021; Romatschke & Houze, 2011; Song & Zhang, 2020). Still, substantial biases exist in simulated diurnal convection in the state-of-the-art global weather and climate models (Baranowski et al., 2019; W.-T. Chen et al., 2019; Dirmeyer et al., 2012; Folkins et al., 2014; Kidd et al., 2013; Love et al., 2011; Ma et al., 2021; Sato et al., 2009; C.-Y. Su et al., 2019; C.-Y. Su, Wu, et al., 2022; Yuan et al., 2013). Only a minor fraction of the latest global storm-resolving models can reasonably reproduce the amplitude and timing of diurnal convection as inferred from satellite observations. For these, additional analyses suggested it being accomplished for incorrect reasons (C.-Y. Su, Chen, et al., 2022). That is, even for high-resolution models in which many critical processes and topography can be resolved, the organization of diurnal convective systems and the convective life

Visualization: Yu-Hung Chang
Writing – original draft: Yu-Hung Chang, Wei-Ting Chen, Yi-Hung Kuo
Writing – review & editing: Yu-Hung Chang, Wei-Ting Chen, Chien-Ming Wu, Yi-Hung Kuo, J. David Neelin

cycle have to be adequately represented. Physical processes characterizing the interactions between local circulation and the thermodynamic environment of convection, especially those that remain under-resolved by global storm-resolving models—including boundary layer turbulence and thermodynamics, local circulation patterns at mountain-valley scales, as well as microphysics—are critical. Orographically-locked precipitation, in addition to being an important phenomenon on its own, can provide a natural laboratory for studying convection where the updrafts and precipitation tend to occur frequently in a particular location. This can facilitate both modeling and potentially the design of field campaigns to examine the inflow of environmental air into the region of active deep convection.

Taiwan, a tropical island with complex topography, is an optimal region to study diurnal convection over complex topography. During summertime, when synoptic-scale weather systems are inactive, rainfall is dominantly produced by diurnal convection (Wang & Chen, 2008). Diurnal convection frequently occurs over specific hotspots on the terrain of Taiwan (Huang et al., 2016; Kuo & Wu, 2019; Lin et al., 2011) when the environmental conditions favor the development of local circulation (land-sea-mountain-valley breeze). Figure 1 displays the conditional probability of summertime diurnal rainfall under weak southwesterly or weak synoptic events classified by the Taiwan Atmospheric Events Database (S.-H. Su et al., 2018). Notable clusters of hotspots can be identified over the northern tip of the Central Mountain Range (magenta box in Figure 1; denoted NCMR hereafter) and the Alishan Mountain Range (southwestern mountains in Taiwan). This prominent feature provides an opportunity to investigate the primary physical processes for the evolution of boundary layer and local circulation associated with orographically-locked diurnal convection over complex topography.

The supply of moisture and energy from the lower troposphere is crucial to the occurrence and maintenance of deep convection (Holloway & Neelin, 2009; Schiro et al., 2016; Tian et al., 2021; Zhang & Klein, 2010). Recent observations identified a typical updraft mass flux structure—for both organized and isolated deep convection—that indicates substantial entrainment of environmental air into the updraft throughout a deep lower-tropospheric layer (Savazzi et al., 2021; Schiro et al., 2018). Such a "deep-inflow" structure implies that the lower-tropospheric layers approximately contributed equally to the estimated conditional instability, consistent with the weighting profile inferred from the observed precipitation-buoyancy relation (Ahmed & Neelin, 2018). The entrainment of environmental air can occur via a coherent inflow or small-scale turbulent mixing (Schiro et al., 2018). The coherent inflow contribution to the dynamical entrainment can be induced by the secondary circulation of organized mesoscale convective systems (Nowotarski et al., 2020) or the local circulation along with boundary layer development (land-sea-mountain-valley breeze).

In regions with complex topography, the path of the inflow associated with diurnally driven convection is often constrained (Barry, 2008; Houze, 2012). Here we hypothesize that the local circulation upon the terrain-constrained inflow path can further augment convection development, strengthening convective activity. This study aims to quantify the importance of the coherent inflow-layer contribution to the convective updraft for orographically-locked diurnal convection in Taiwan. To identify key physical processes, we conduct an ensemble of large-eddy simulations (LESs) implemented with realistic, high-resolution topography of Taiwan, subject to weak synoptic conditions favorable for the development of diurnal local circulation.

This manuscript is organized as follows. Section 2 reveals the simulation configuration details and how the deep-inflow features are identified and analyzed. The analysis for diurnal convection over complex topography is presented in Section 3, including the convective updraft structure and the circulation pattern of moist static energy (MSE) transport. Section 4 discusses the preliminary observational results of the deep-inflow layer from the initial field measurements guided by the analysis of the LESs. The discussion and summary are in Section 5.

2. Methodology

2.1. Model and Simulation Configuration

For this study, we used the vector vorticity equation cloud-resolving model (VVM; Jung & Arakawa, 2008) with high-resolution Taiwan topography and land-use types, named TaiwanVVM (Wu et al., 2019). The horizontal resolution is 500 m and the domain size is 512 km × 512 km. The length of the simulations is 24 hr, starting from 00:00 (i.e., midnight) through 24:00, which is tied to the local insolation cycle. Since the land-atmosphere coupling is noted to be an essential component for convective development in TaiwanVVM, the Noah land surface model (Noah LSM; F. Chen & Dudhia, 2001; F. Chen et al., 1996) version 3.4.1 is coupled to the model; The top soil layers for all land grids are initialized using the daily average soil moisture over the island of

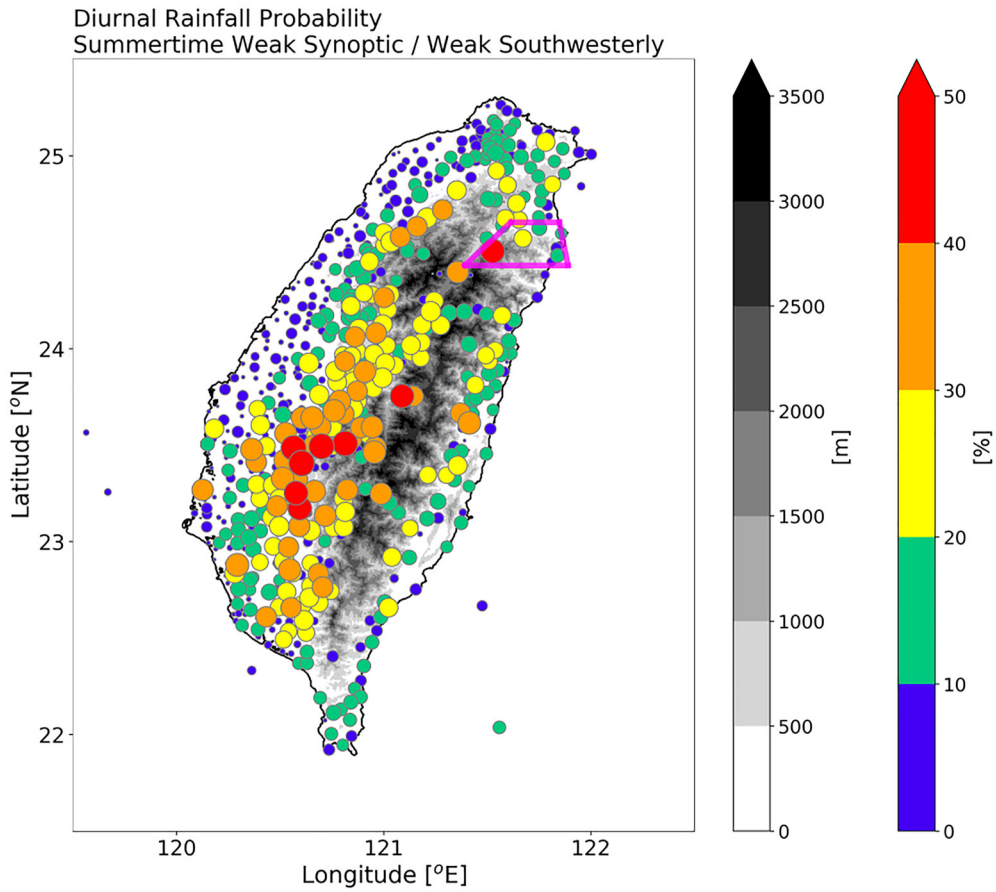

Figure 1. The topography of Taiwan (gray shading) and conditional probability (colored dots) of summertime diurnal rainfall under the weak synoptic or weak southwesterly events. To find the days with a prominent diurnal precipitation cycle, only the days with precipitation in the afternoon greater than that in the morning and with the peak rainfall occurring in the afternoon are selected. The threshold of the hourly accumulated rainfall is at least 0.5 mm. The precipitation is from the Central Weather Bureau hourly rain gauge data from 1993 through 2020 (Data Bank for Atmospheric and Hydrologic Research, 2023). For visual clarity, the area of colored dots is proportional to the probability. The magenta box marks the northern end of the Central Mountain Range area (NCMR) on which subsequent analyses are focused.

Taiwan from the Global Land Data Assimilation System (GLDAS; Rodell et al., 2004) version 2.0. In the VVM formulation the pressure gradient force is eliminated, and the vorticity field—driven by horizontal buoyancy gradient—directly responds to surface fluxes. This makes TaiwanVVM advantageous to simulate local circulation driven by differential surface heating over complex, steep topography; aerosol effect on diurnal convection (Chang et al., 2021); and air pollutant transport affected by lee vortex and boundary layer development (Hsieh et al., 2022; Hsu et al., 2023).

The TaiwanVVM LES ensemble analyzed here has been documented in Chang et al. (2021). The ensemble consists of 30 cases selected to cover the environmental variability of the summertime weak synoptic weather regime that favors local circulation development. The observed soundings are simplified as the uniform initial condition over the entire domain, commonly used in LESs (e.g., Grabowski et al., 2006), to emphasize the decisive environmental factors that modulate the development of convection, while the ensemble members represent the variability of these environmental factors. In such a "semi-realistic" approach, the evolution of local circulation and convection is dominated by interactions among physical processes.

2.2. Deep Convective Columns and Their Convective Parameters

The magenta box in Figure 1 is selected to focus on precipitation hotspots. We impose criteria on the rain rate and vertical velocity to ensure the sampling of deep convective columns over precipitation hotspots. Each ensemble

member's 99th percentile of the rain rate in the NCMR area is defined as the critical rain rate of that simulation. The largest contiguous grids that once experienced rainfall greater than the critical rain rate of its simulation would be determined as the precipitation hotspot. Inside the precipitation hotspot, atmospheric columns with a mean vertical velocity between 3 and 10 km greater than 1 m s^{-1} are further identified as deep convective columns. This criterion upon vertical velocity is less strict than those in Schiro et al. (2018), so the precipitating columns with mild low-level downdraft can still be included, preserving the simultaneous existence of precipitation and upward motion in general. In all 30 semi-realistic ensemble members, 25 simulations have wide enough deep convective columns in the NCMR area, whose critical rain rates range from 15.16 to 74.99 mm.

Aside from identifying deep convective columns through rain rate and vertical velocity, distinguishing the surroundings of deep convective columns further helps us to conceptualize the deep-inflow mixing of deep convective columns over complex topography. To diagnose the buoyancy characteristics of deep convective columns, we define the environment of the precipitation hotspot. It is a square area centered at the centroid of the precipitation hotspot, whose side length is six-fold the effective radius of the precipitation hotspot. Furthermore, we determine the cross-section profile of the deep-inflow by the upstream vector to explore the circulation patterns of deep convective columns and their deep-inflow. The upstream vector is defined as the mean integrated vapor transport in the environment of the precipitation hotspot below 2 km and within 2 hr before rain initiation.

The buoyancy of deep convective columns can contribute to the tendency of vertical velocity. It is calculated from $B = g(\theta_v - \theta_{v,\mathrm{env}})/\theta_{v,\mathrm{env}}$, where g is the gravitational acceleration, θ_v is the virtual potential temperature of deep convective columns, and $\theta_{v,\mathrm{env}}$ is the mean virtual potential temperature of the environment. The convective mass flux of deep convective columns can be translated from vertical velocity, representing the upward transport of air mass. It is calculated from $m = \rho\sigma w$, where ρ is the mean air density of deep convective columns, σ is the fraction of deep convective columns covered by updrafts, and w is the mean vertical velocity of deep convective columns.

3. Results

In this section, we examine orographically-locked diurnal convection using the deep-inflow mixing framework following Schiro et al. (2018). The convective updraft mass flux profile provides evidence for deep-inflow mixing. Thus, the analyses of convective structures are displayed. Since diurnal convection is orographically-locked, the deep-inflow can be analyzed in the physical space relative to a specific deep-inflow path. The concept of deep-inflow mixing is further extended to characterize the upstream MSE transport via local circulation.

3.1. Convective Structures

Schiro et al. (2018) depicted an increasing convective mass flux with height in the lower troposphere, indicating the characteristic of deep-inflow mixing. The buoyancy, vertical velocity, and convective mass flux profiles of deep convective columns in all simulations are illustrated in Figures 2a–2c (black lines), representing the convective structures. The profiles of these deep convective columns have a common shape with substantial variability in updraft intensity. The mean buoyancy of deep convective columns is positive between 0.45 and 10.73 km, reaching its peak of 2.62×10^{-2} m s^{-2} at 5.22 km. Since buoyancy represents the tendency of vertical motion, we suppose an accelerated updraft with height inside deep convective columns, and the peak of the mean vertical velocity appears at a higher altitude than the mean buoyancy. As expected, the mean vertical velocity of deep convective columns increases with height, reaching its peak of 3.80 m s^{-1} at 6.23 km. The convective mass flux, which is related to the mean vertical velocity and the updraft fraction in deep convective columns, also shows an increase with height in the lower troposphere. The mean convective mass flux of deep convective columns reaches the peak of 1.95×10^2 g m^{-2} s^{-1} at 5.53 km. Since deep convective columns usually occur over topography higher than 1.6 km, the vertical structure at low levels could be influenced by the terrain, showing values of approximately zero. The increasing convective mass flux with height in the lower troposphere, providing positive buoyancy, indicates a deep layer of environmental air flows into the updraft of deep convective columns.

The deep-inflow mixing reveals the influence of the environment on convection. Thus, the influence function is utilized to quantify the contribution from different layers. The formulation of the influence function can be approximated by $I(z_B, z) = \frac{1}{m(z_B)}\frac{\partial m(z)}{\partial z}$ (Schiro et al., 2018), which is the vertical rate of change for convective mass flux normalized by the convective mass flux of the reference level (z_B). This approximation is valid only for $\frac{\partial m(z)}{\partial z} > 0$, provided there is no detrainment. For the height of the maximum convective mass flux ($z_B = 5.53$ km)

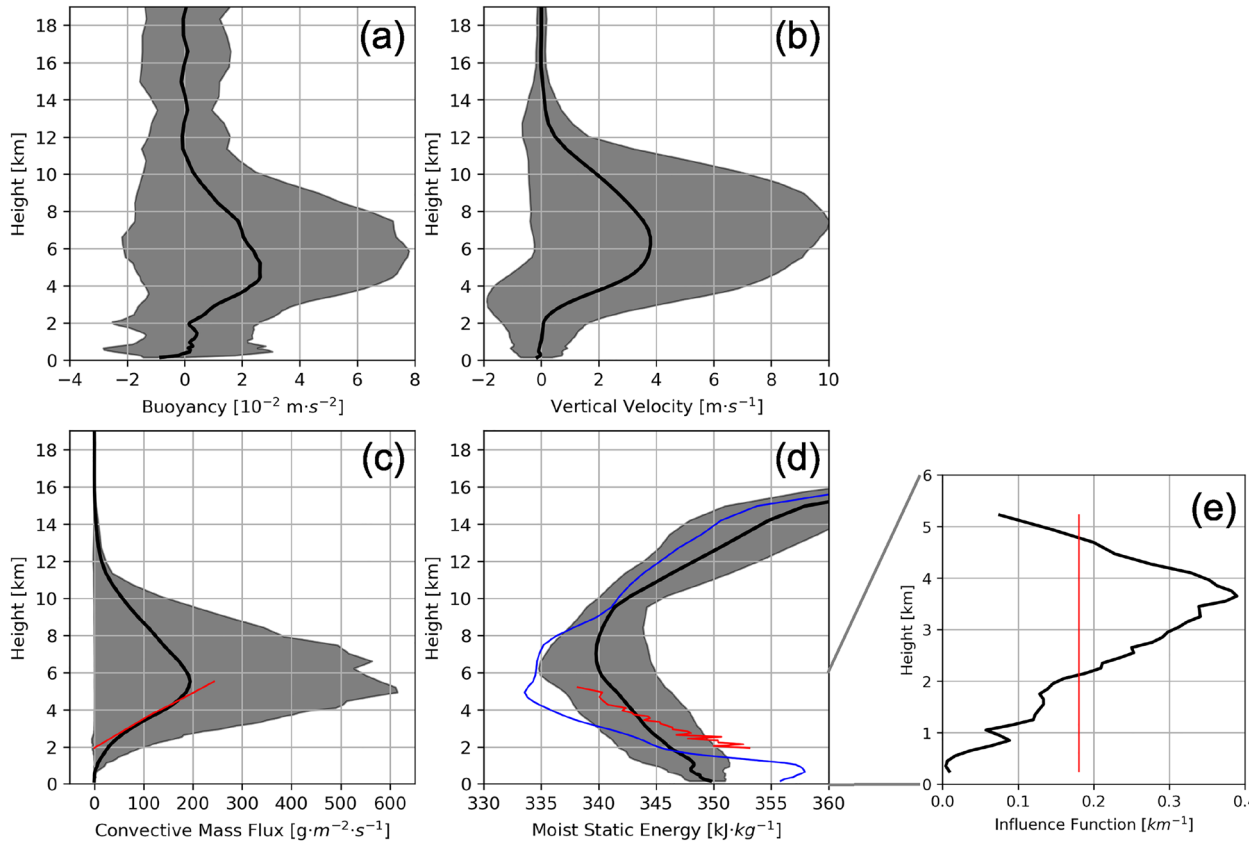

Figure 2. The profiles of (a) buoyancy, (b) vertical velocity, (c) convective mass flux, and (d) moist static energy (MSE) of deep convective columns in NCMR. The solid black lines represent the mean values, and the gray shadings are between the 10th and 90th percentile. (e) The influence function calculated by the mean convective mass flux following Schiro et al. (2018) focused on the lower troposphere. Note the different *y*-axis. The red line in (e) is the idealized constant influence function with the same value. The red lines in (c) and (d) are the profiles calculated using this constant influence function. The blue line in (d) is the upstream MSE.

used as the reference, the influence function has variation in height and peaks around 3.65 km (Figure 2e). For a theoretical linear dependence of convective mass flux with height, an approximation of a constant influence function $I = z_B^{-1} \simeq 0.18$ km^{-1} can be made. This theoretical convective mass flux is displayed by the red line in Figure 2c, with the initial level (z_i) being the lowest level of continuous increase in buoyancy with height (1.95 km). The theoretical convective mass flux corresponds well with the mean convective mass flux of deep convective columns, indicating that the approximation is reasonable.

Figure 2d displays the mean MSE of deep convective columns (black line), the mean MSE of upstream (blue line), and the theoretical MSE calculated by the constant influence function (red line). The theoretical MSE is calculated from $\text{MSE} = \int_{z_i}^{z_B} \text{MSE}_{\text{env}} I(z_B, z) dz$, representing the contribution of upstream MSE transport of each layer from the deep-inflow. The theoretical MSE has little difference compared with the mean MSE of deep convective columns, indicating that the contribution from the pre-existing local MSE in the deep convective columns is limited. Nevertheless, the feature of upstream MSE transport provides sufficient evidence of deep-inflow mixing via local circulation in TaiwanVVM simulations.

3.2. Upstream MSE Transport

For diurnal convection developed randomly over great plains (e.g., the Amazon), the inflow can come from all directions, making it challenging to clarify the direction of the inflow and illustrate the circulation patterns. Since diurnal convection over complex topography is orographically-locked, we can demonstrate the deep-inflow mixing features by not only the convective structures but also the circulation patterns of the deep-inflow. Figures 3a–3d show the circulation pattern of the deep-inflow of an ensemble member as an example case. In Figure 3a, the blue

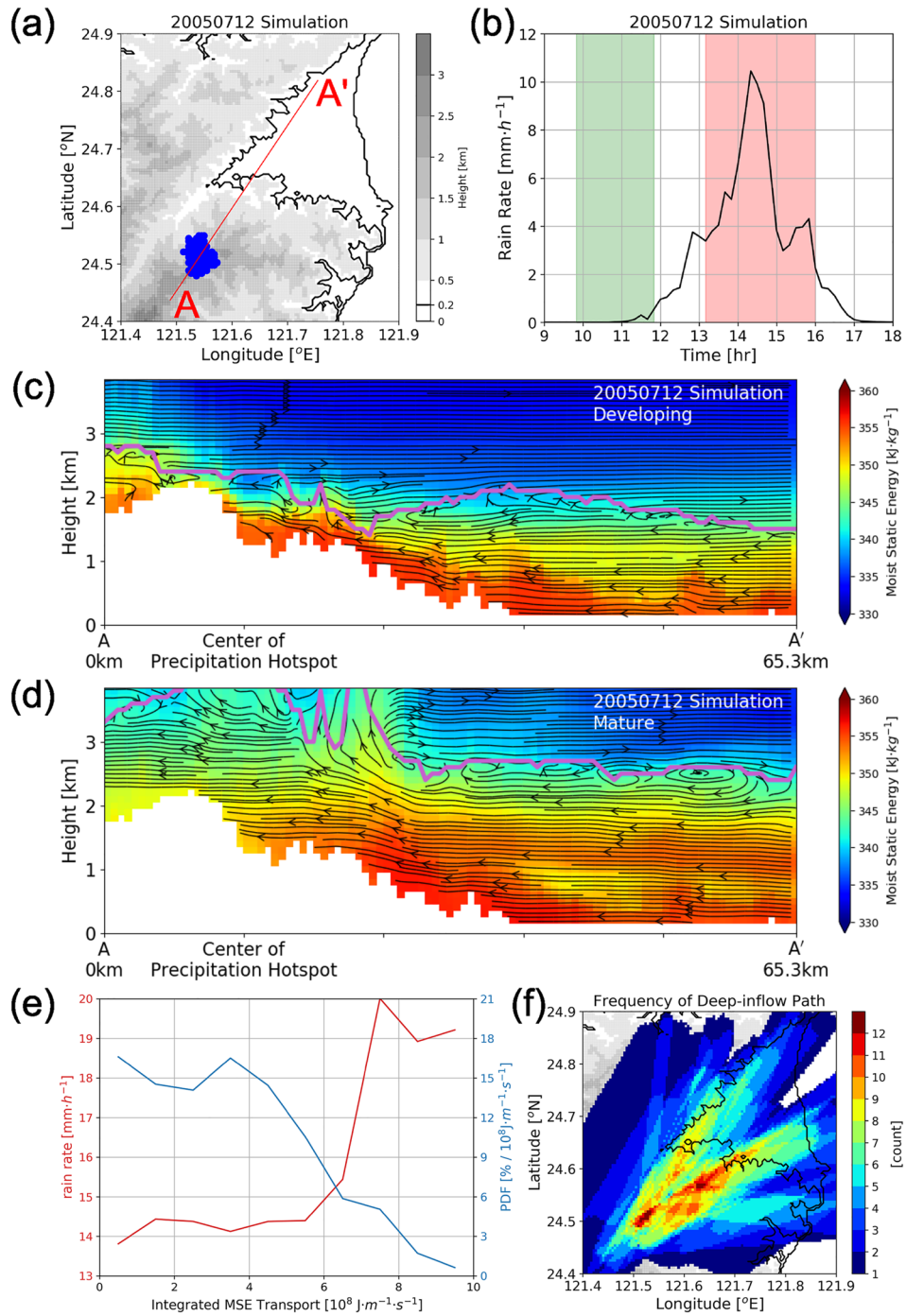

Figure 3. (a) The precipitation hotspot (blue area) and the cross-section line determined by the upstream vector (red line) in a case simulation (20050712). The gray shading is the topography. (b) The mean rain rate evolution in the NCMR area of this case simulation. The green and red shadings represent the developing and mature stages, respectively. (c), (d) The composite cross-section profile of moist static energy (MSE) (color shading) and circulation (streamline) of this case simulation for the developing stage and the mature stage. The purple lines represent the top of the inflow layer. (e) The relationship between the upstream integrated MSE transport during the developing stage and the mean rain rate in the precipitation hotspot during the mature stage (red). The probability density function of the upstream integrated MSE transport during the developing stage (blue). (f) The frequency of the deep-inflow in the 25 cases with deep convective columns. The gray shading is the topography as in (a).

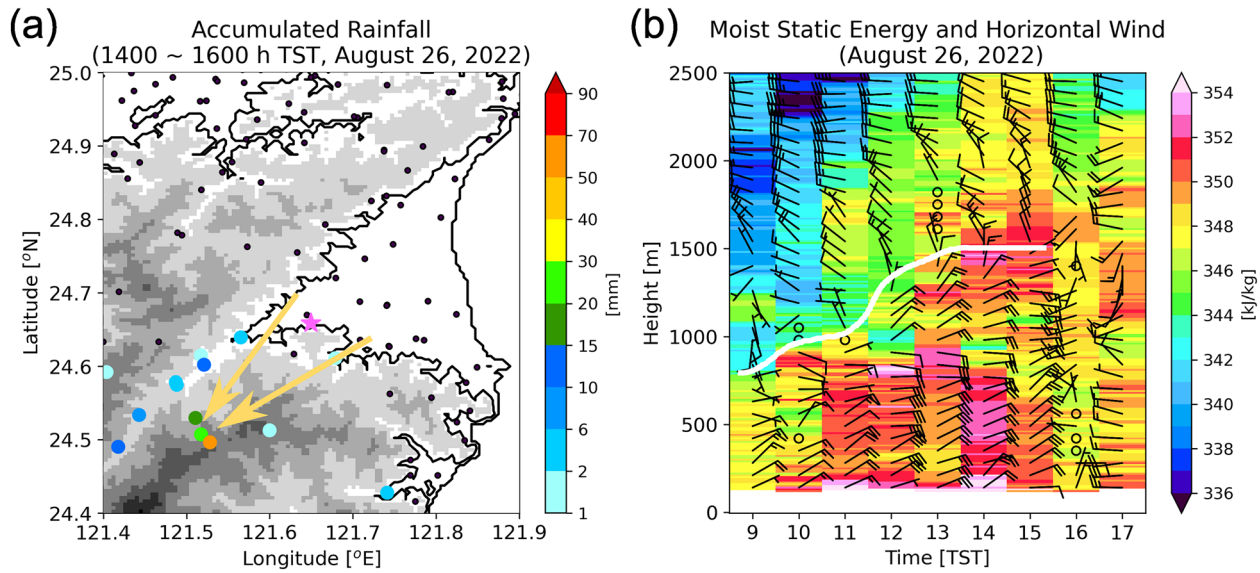

Figure 4. (a) The accumulated rainfall recorded by automatic weather stations (colored dots) during 14:00–16:00 hr Taiwan Standard Time on 26 August 2022. The black dots are stations with no recorded rainfall in this period. The gray shading is the topography as in Figure 3a. The yellow arrows represent the frequent paths of the deep-inflow identified in Figure 3f. (b) The moist static energy and horizontal wind observed hourly at Sunsing [indicated by the magenta star in (a)] on the same day, using the Storm Tracker mini-radiosondes (Hwang et al., 2020). The solid white line signifies the top of the northeasterly layer.

area is the precipitation hotspot of this example case, and the red cross-section line, determined by the upstream vector defined in Section 2.2, passes through the centroid of the precipitation hotspot, portraying the deep-inflow path. Figures 3c and 3d illustrate the composite profile of the cross-section line during the developing stage and the mature stage of the example case. The developing stage (green shading period in Figure 3b) is within 2 hr before the mean rain rate in the NCMR area surpasses 0.5 mm hr^{-1}, while the mature stage (red shading period in Figure 3b) is when deep convective columns appear. During the developing stage, an inflow layer below 2.0 km depth transports MSE from the plain toward the mountains. The averaged upstream MSE flux below 2 km is 5.44×10^5 J m^{-2} s^{-1}. The surface heating and the turbulent mixing in the boundary layer result in the development and thickening of the inflow layer. During the mature stage, diurnal convection develops near the center of the precipitation hotspot. The depth of the inflow layer is about 2.6 km, accompanied by the averaged upstream MSE flux below 2 km of 7.71×10^5 J m^{-2} s^{-1}.

The high MSE transport is the prominent feature of the deep-inflow mixing from the perspective of circulation patterns. Figures 3c and 3d reveal that the MSE transport during the developing stage can contribute to the growth of diurnal convection, which is further supported by the statistics in Figure 3e. As the upstream integrated MSE transport during the developing stage rises from below 6×10^8 J m^{-1} s^{-1} to exceeding 7×10^8 J m^{-1} s^{-1}, the mean rain rate in the precipitation hotspot during the mature stage increases from 14.25 to 19.38 mm hr^{-1}. That is, enhanced upstream integrated MSE transport during the developing stage leads to a 36% increment in the mean rain rate in the precipitation hotspots during the mature stage. The results highlight the importance of non-local dynamical entrainment of the deep-inflow, transporting MSE via local circulation to supply the growth of orographically-locked diurnal convection.

4. Field Observation Guided by Simulations

The circulation pattern of the deep-inflow mixing and the accompanied upstream MSE transport can be identified in the TaiwanVVM simulations. Furthermore, the statistics from the TaiwanVVM semi-realistic LES ensembles provide helpful guidance for deploying boundary layer observations. Figure 3f shows the frequency of the deep-inflow. Two frequent paths, simplified by the yellow arrows in Figure 4a, are located over the two river valleys. At Sunsing (the magenta star in Figure 4a), a location over the foothill with a high frequency of the deep-inflow path, we released the Storm Tracker (ST) mini-radiosondes to observe the evolution of the deep-inflow. The ST mini-radiosonde is a compact, light-weight, economical, and well-calibrated sensor (Hwang et al., 2020), and it has been utilized in the Yilan Experiment of Severe Rainfall (YESR2020) field campaign

(S.-H. Su et al., 2022). An observation was conducted on 26 August 2022. This afternoon, Taipingshan Station (CWB station number 01U560) in the NCMR area recorded 59.0 mm in 2 hr (Figure 4a). Figure 4b displays the evolution of MSE and horizontal wind observed by the ST mini-radiosondes. The depth of the low-level northeasterly increased from 09:00 to 15:00 Taiwan Standard Time (TST, UTC+8), revealing the evolution of the inflow layer. The MSE in the inflow layer also increased with time, reaching its maximum at 14:00 TST, just before the maximum rainfall occurred at Taipingshan Station. The observational evidence demonstrated the high MSE transport by the deep-inflow toward the precipitation hotspot.

5. Discussion and Summary

This study focuses on regions with high occurrence of strong convection, that is, precipitation hotspots, over mountains under weak synoptic weather regime during summertime in Taiwan. Such a weather regime favors the development of local land-sea-mountain-valley-breeze circulation driven by differential surface heating over steep topography. A TaiwanVVM LES ensemble is simulated with the realistic, complex topography of Taiwan and initiated using a set of radiosonde observations to span the variability of the background environment. In this ensemble, through mass continuity, a deep layer of inflow can be inferred from the common mass flux structure of strong updrafts—the mass flux increasing gradually with height throughout the lower troposphere—identified during heavy precipitation over the hotspots. Furthermore, a deep layer (including the boundary layer) of coherent inflow air can be directly identified in the simulations with elevated MSE transport along its path. The orographically-locked diurnal convection over the hotspot is enhanced by the high upstream MSE transport, leading to an averaged 36% increase in rain rate.

The presence of orographically-locked convection provides a unique opportunity for studying convective updrafts and precipitation—because the typical location of the updraft is geographically constrained, field measurements can be more easily placed to sample the environment likely to influence the convection. A field campaign on 26 August 2022, guided by the simulations, released the ST mini-radiosondes (Hwang et al., 2020) to quantify the upstream environment of the most common deep-inflow path. The initial analysis supports the existence of high MSE transport within the inflow layer when organized convection occurs over the region of precipitation hotspot. While aspects of this flow may be specific to the orographic conditions, the presence of the deep inflow layer is consistent with and reinforces other lines of evidence (Ahmed & Neelin, 2018; Derbyshire et al., 2004; Holloway & Neelin, 2009; Houze, 2004, 2018; Nicolas & Boos, 2022; Nowotarski et al., 2020; Schiro et al., 2018) that the other properties of deep convection may also be examined in the upcoming field observations motivated by the analyses in the present study.

Data Availability Statement

The analyzing codes and post-processing data are available in the online open-access repositories (https://doi.org/10.6084/m9.figshare.21986564 and https://doi.org/10.6084/m9.figshare.21986900).

Acknowledgments
This research is jointly supported by the National Science and Technology Council of Taiwan through Grants NSTC-110-2123-M-002-007, NSTC-109-2628-M-002-003-MY3, and NSTC-111-2111-M-002-012 and National Taiwan University Grants NTU-112L7832 and NTU-112L7858 (YHC, WTC, and CMW). We extend our heartfelt gratitude to the research assistants and students who contributed to the field campaign by engaging in discussions, making measurements, providing logistical support, and handling administrative tasks. The NTU COOK lab and Mr. Chi-Bao Fu are recognized for their indispensable equipment and services. Additionally, we acknowledge Dr. An-Hsiang Wang for his efforts in curating the data from the Central Weather Bureau surface observation. JDN and YHK were supported under National Science Foundation AGS-1936810 and National Oceanic and Atmospheric Administration NA21OAR4310354. YHK was also supported under NA18OAR4320123 from the National Oceanic and Atmospheric Administration, U.S. Department of Commerce. The statements, findings, conclusions, and recommendations are those of the author(s) and do not necessarily reflect the views of the National Oceanic and Atmospheric Administration, or the U.S. Department of Commerce.

References

Ahmed, F., & Neelin, J. D. (2018). Reverse engineering the tropical precipitation–buoyancy relationship. *Journal of the Atmospheric Sciences*, *75*(5), 1587–1608. https://doi.org/10.1175/jas-d-17-0333.1

Baranowski, D. B., Waliser, D. E., Jiang, X., Ridout, J. A., & Flatau, M. K. (2019). Contemporary GCM fidelity in representing the diurnal cycle of precipitation over the Maritime Continent. *Journal of Geophysical Research: Atmospheres*, *124*(2), 747–769. https://doi.org/10.1029/2018JD029474

Barry, R. G. (2008). Geographical controls of mountain meteorological elements. In R. G. Barry (Ed.), *Mountain weather and climate* (3 ed., pp. 24–124). Cambridge University Press. https://doi.org/10.1017/CBO9780511754753.003

Chang, Y.-H., Chen, W.-T., Wu, C.-M., Moseley, C., & Wu, C.-C. (2021). Tracking the influence of cloud condensation nuclei on summer diurnal precipitating systems over complex topography in Taiwan. *Atmospheric Chemistry and Physics*, *21*(22), 16709–16725. https://doi.org/10.5194/acp-21-16709-2021

Chen, F., & Dudhia, J. (2001). Coupling an advanced land surface–hydrology model with the Penn State–NCAR MM5 modeling system. Part I: Model implementation and sensitivity. *Monthly Weather Review*, *129*(4), 569–585. https://doi.org/10.1175/1520-0493(2001)129<0569:CAALSH>2.0.CO;2

Chen, F., Mitchell, K., Schaake, J., Xue, Y., Pan, H.-L., Koren, V., et al. (1996). Modeling of land surface evaporation by four schemes and comparison with FIFE observations. *Journal of Geophysical Research*, *101*(D3), 7251–7268. https://doi.org/10.1029/95JD02165

Chen, P.-J., Chen, W.-T., Wu, C.-M., & Yo, T.-S. (2021). Convective cloud regimes from a classification of object-based CloudSat observations over Asian-Australian monsoon areas. *Geophysical Research Letters*, *48*(10), e2021GL092733. https://doi.org/10.1029/2021GL092733

Chen, W.-T., Wu, C.-M., & Ma, H.-Y. (2019). Evaluating the bias of South China Sea summer monsoon precipitation associated with fast physical processes using a climate model hindcast approach. *Journal of Climate*, *32*(14), 4491–4507. https://doi.org/10.1175/jcli-d-18-0660.1

Chen, X., Zhao, K., Xue, M., Zhou, B., Huang, X., & Xu, W. (2015). Radar-observed diurnal cycle and propagation of convection over the Pearl River Delta during Mei-Yu season. *Journal of Geophysical Research: Atmospheres*, *120*(24), 12557–12575. https://doi.org/10.1002/2015JD023872

Data Bank for Atmospheric and Hydrologic Research. (2023). Central Weather Bureau surface observation [Dataset]. Department of Atmospheric Sciences, Chinese Culture University. Retrieved from http://dbar.pccu.edu.tw/

Derbyshire, S. H., Beau, I., Bechtold, P., Grandpeix, J.-Y., Piriou, J.-M., Redelsperger, J.-L., & Soares, P. M. M. (2004). Sensitivity of moist convection to environmental humidity. *Quarterly Journal of the Royal Meteorological Society*, *130*(604), 3055–3079. https://doi.org/10.1256/qj.03.130

Dirmeyer, P. A., Cash, B. A., Kinter, J. L., Jung, T., Marx, L., Satoh, M., et al. (2012). Simulating the diurnal cycle of rainfall in global climate models: Resolution versus parameterization. *Climate Dynamics*, *39*(1), 399–418. https://doi.org/10.1007/s00382-011-1127-9

Folkins, I., Mitovski, T., & Pierce, J. R. (2014). A simple way to improve the diurnal cycle in convective rainfall over land in climate models. *Journal of Geophysical Research: Atmospheres*, *119*(5), 2113–2130. https://doi.org/10.1002/2013JD020149

Grabowski, W. W., Bechtold, P., Cheng, A., Forbes, R., Halliwell, C., Khairoutdinov, M., et al. (2006). Daytime convective development over land: A model intercomparison based on LBA observations. *Quarterly Journal of the Royal Meteorological Society*, *132*(615), 317–344. https://doi.org/10.1256/qj.04.147

Holloway, C. E., & Neelin, J. D. (2009). Moisture vertical structure, column water vapor, and tropical deep convection. *Journal of the Atmospheric Sciences*, *66*(6), 1665–1683. https://doi.org/10.1175/2008jas2806.1

Houze, R. A. (2004). Mesoscale convective systems. *Reviews of Geophysics*, *42*(4). https://doi.org/10.1029/2004RG000150

Houze, R. A. (2012). Orographic effects on precipitating clouds. *Reviews of Geophysics*, *50*(1). https://doi.org/10.1029/2011RG000365

Houze, R. A. (2018). 100 years of research on mesoscale convective systems. *Meteorological Monographs*, *59*, 17.1–17.54. https://doi.org/10.1175/AMSMONOGRAPHS-D-18-0001.1

Hsieh, M.-K., Chen, Y.-W., Chen, Y.-C., & Wu, C.-M. (2022). The roles of local circulation and boundary layer development in tracer transport over complex topography in central Taiwan. *Journal of the Meteorological Society of Japan*, *100*(3), 555–573. https://doi.org/10.2151/jmsj.2022-028

Hsu, T.-H., Chen, W.-T., Wu, C.-M., & Hsieh, M.-K. (2023). The observation-based index to investigate the role of the lee vortex in enhancing air pollution over northwestern Taiwan. *Journal of Applied Meteorology and Climatology*, *62*(3), 427–439. https://doi.org/10.1175/jamc-d-22-0102.1

Huang, W.-R., Chang, Y.-H., Hsu, H.-H., Cheng, C.-T., & Tu, C.-Y. (2016). Dynamical downscaling simulation and future projection of summer rainfall in Taiwan: Contributions from different types of rain events. *Journal of Geophysical Research: Atmospheres*, *121*(23), 13973–13988. https://doi.org/10.1002/2016JD025643

Hwang, W.-C., Lin, P.-H., & Yu, H. (2020). The development of the "Storm Tracker" and its applications for atmospheric high-resolution upper-air observations. *Atmospheric Measurement Techniques*, *13*(10), 5395–5406. https://doi.org/10.5194/amt-13-5395-2020

Jian, H.-W., Chen, W.-T., Chen, P.-J., Wu, C.-M., & Rasmussen, K. L. (2021). The synoptically-influenced extreme precipitation systems over Asian-Australian monsoon region observed by TRMM precipitation radar. *Journal of the Meteorological Society of Japan*, *99*(2), 269–285. https://doi.org/10.2151/jmsj.2021-013

Jung, J.-H., & Arakawa, A. (2008). A three-dimensional anelastic model based on the vorticity equation. *Monthly Weather Review*, *136*(1), 276–294. https://doi.org/10.1175/2007mwr2095.1

Kidd, C., Dawkins, E., & Huffman, G. (2013). Comparison of precipitation derived from the ECMWF operational forecast model and satellite precipitation datasets. *Journal of Hydrometeorology*, *14*(5), 1463–1482. https://doi.org/10.1175/jhm-d-12-0182.1

Krishna, U. V. M., Das, S. K., Deshpande, S. M., & Pandithurai, G. (2021). Physical processes controlling the diurnal cycle of convective storms in the Western Ghats. *Scientific Reports*, *11*(1), 14103. https://doi.org/10.1038/s41598-021-93173-0

Kuo, K.-T., & Wu, C.-M. (2019). The precipitation hotspots of afternoon thunderstorms over the Taipei Basin: Idealized numerical simulations. *Journal of the Meteorological Society of Japan*, *97*(2), 501–517. https://doi.org/10.2151/jmsj.2019-031

Lin, P.-F., Chang, P.-L., Jou, B. J.-D., Wilson, J. W., & Roberts, R. D. (2011). Warm season afternoon thunderstorm characteristics under weak synoptic-scale forcing over Taiwan Island. *Weather and Forecasting*, *26*(1), 44–60. https://doi.org/10.1175/2010waf2222386.1

Love, B. S., Matthews, A. J., & Lister, G. M. S. (2011). The diurnal cycle of precipitation over the Maritime Continent in a high-resolution atmospheric model. *Quarterly Journal of the Royal Meteorological Society*, *137*(657), 934–947. https://doi.org/10.1002/qj.809

Ma, H.-Y., Zhou, C., Zhang, Y., Klein, S. A., Zelinka, M. D., Zheng, X., et al. (2021). A multi-year short-range hindcast experiment with CESM1 for evaluating climate model moist processes from diurnal to interannual timescales. *Geoscientific Model Development*, *14*(1), 73–90. https://doi.org/10.5194/gmd-14-73-2021

Nesbitt, S. W., & Zipser, E. J. (2003). The diurnal cycle of rainfall and convective intensity according to three years of TRMM measurements. *Journal of Climate*, *16*(10), 1456–1475. https://doi.org/10.1175/1520-0442(2003)016<1456:TDCORA>2.0.CO;2

Nicolas, Q., & Boos, W. R. (2022). A theory for the response of tropical mist convection to mechanical orographic forcing. *Journal of the Atmospheric Sciences*, *79*(7), 1761–1779. https://doi.org/10.1175/JAS-D-21-0218.1

Nowotarski, C. J., Peters, J. M., & Mulholland, J. P. (2020). Evaluating the effective inflow layer of simulated supercell updrafts. *Monthly Weather Review*, *148*(8), 3507–3532. https://doi.org/10.1175/MWR-D-20-0013.1

Rodell, M., Houser, P. R., Jambor, U., Gottschalck, J., Mitchell, K., Meng, C.-J., et al. (2004). The global land data assimilation system. *Bulletin of the American Meteorological Society*, *85*(3), 381–394. https://doi.org/10.1175/BAMS-85-3-381

Romatschke, U., & Houze, R. A. (2011). Characteristics of precipitating convective systems in the South Asian monsoon. *Journal of Hydrometeorology*, *12*(1), 3–26. https://doi.org/10.1175/2010JHM1289.1

Sato, T., Miura, H., Satoh, M., Takayabu, Y. N., & Wang, Y. (2009). Diurnal cycle of precipitation in the tropics simulated in a global cloud-resolving model. *Journal of Climate*, *22*(18), 4809–4826. https://doi.org/10.1175/2009jcli2890.1

Savazzi, A. C. M., Jakob, C., & Siebesma, A. P. (2021). Convective mass-flux from long term radar reflectivities over Darwin, Australia. *Journal of Geophysical Research: Atmospheres*, *126*(19), e2021JD034910. https://doi.org/10.1029/2021JD034910

Schiro, K. A., Ahmed, F., Giangrande, S. E., & Neelin, J. D. (2018). GoAmazon2014/5 campaign points to deep-inflow approach to deep convection across scales. *Proceedings of the National Academy of Sciences of the United States of America*, *115*(18), 4577–4582. https://doi.org/10.1073/pnas.1719842115

Schiro, K. A., Neelin, J. D., Adams, D. K., & Lintner, B. R. (2016). Deep convection and column water vapor over tropical land versus tropical ocean: A comparison between the Amazon and the tropical Western Pacific. *Journal of the Atmospheric Sciences*, *73*(10), 4043–4063. https://doi.org/10.1175/jas-d-16-0119.1

Song, Z., & Zhang, J. (2020). Diurnal variations of summer precipitation linking to the topographical conditions over the Beijing-Tianjin-Hebei region. *Scientific Reports*, *10*(1), 9701. https://doi.org/10.1038/s41598-020-65743-1

Su, C.-Y., Chen, W.-T., Wu, C.-M., & Ma, H.-Y. (2022). Object-Based evaluation of tropical precipitation systems in DYAMOND simulations over the Maritime Continent. *Journal of the Meteorological Society of Japan*, *100*(4), 647–659. https://doi.org/10.2151/jmsj.2022-033

Su, C.-Y., Wu, C.-M., Chen, W.-T., & Chen, J.-H. (2019). Object-based precipitation system bias in grey zone simulation: The 2016 South China Sea summer monsoon onset. *Climate Dynamics*, *53*(1), 617–630. https://doi.org/10.1007/s00382-018-04607-x

Su, C.-Y., Wu, C.-M., Chen, W.-T., & Chen, J.-H. (2022). The effects of the unified parameterization in the CWBGFS: The diurnal cycle of precipitation over land in the Maritime Continent. *Climate Dynamics*, *58*(1), 223–233. https://doi.org/10.1007/s00382-021-05899-2

Su, S.-H., Chang, Y.-H., Liu, C.-H., Chen, W.-T., Chang, W.-Y., Chen, J.-P., et al. (2022). Observing severe precipitation near complex topography during the Yilan Experiment of Severe Rainfall in 2020 (YESR2020). *Quarterly Journal of the Royal Meteorological Society*, *148*(745), 1663–1682. https://doi.org/10.1002/qj.4271

Su, S.-H., Chu, J.-L., Yo, T.-S., & Lin, L.-Y. (2018). Identification of synoptic weather types over Taiwan area with multiple classifiers. *Atmospheric Science Letters*, *19*(12), e861. https://doi.org/10.1002/asl.861

Tian, Y., Zhang, Y., Klein, S. A., & Schumacher, C. (2021). Interpreting the diurnal cycle of clouds and precipitation in the ARM GoAmazon observations: Shallow to deep convection transition. *Journal of Geophysical Research: Atmospheres*, *126*(5), e2020JD033766. https://doi.org/10.1029/2020JD033766

Wang, S.-Y., & Chen, T.-C. (2008). Measuring East Asian summer monsoon rainfall contributions by different weather systems over Taiwan. *Journal of Applied Meteorology and Climatology*, *47*(7), 2068–2080. https://doi.org/10.1175/2007jamc1821.1

Wu, C.-M., Lin, H.-C., Cheng, F.-Y., & Chien, M.-H. (2019). Implementation of the land surface processes into a vector vorticity equation model (VVM) to study its impact on afternoon thunderstorms over complex topography in Taiwan. *Asia-Pacific Journal of Atmospheric Sciences*, *55*(4), 701–717. https://doi.org/10.1007/s13143-019-00116-x

Yang, G.-Y., & Slingo, J. (2001). The diurnal cycle in the tropics. *Monthly Weather Review*, *129*(4), 784–801. https://doi.org/10.1175/1520-0493(2001)129<0784:TDCITT>2.0.CO;2

Yuan, W., Yu, R., Zhang, M., Lin, W., Li, J., & Fu, Y. (2013). Diurnal cycle of summer precipitation over subtropical East Asia in CAM5. *Journal of Climate*, *26*(10), 3159–3172. https://doi.org/10.1175/jcli-d-12-00119.1

Zhang, Y., & Klein, S. A. (2010). Mechanisms affecting the transition from shallow to deep convection over land: Inferences from observations of the diurnal cycle collected at the ARM Southern Great Plains site. *Journal of the Atmospheric Sciences*, *67*(9), 2943–2959. https://doi.org/10.1175/2010jas3366.1